alloys

MDPI

Article

Anomalous Work Hardening Behavior of a Single Crystalline Co-Base Superalloy

Andreas Bezold [1,*], Nicklas Volz [1], Fei Xue [2], Mathias Göken [1] and Steffen Neumeier [1]

[1] Department of Materials Science & Engineering, Institute I: General Materials Properties, Friedrich-Alexander-Universität Erlangen-Nürnberg, D-91058 Erlangen, Germany
[2] Department of Materials Science and Engineering, University of Michigan, Ann Arbor, MI 48109, USA
* Correspondence: andreas.bezold@fau.de

Abstract: The defect evolution associated with an anomalous work hardening behavior of a single crystalline quaternary Co-Al-W-Ta superalloy at 950 °C was investigated by transmission electron microscopy. As plastic deformation is initially confined to the γ matrix channels, a plateau arises in the stress-strain curve after yielding. At about 1% plastic strain, extensive shearing of the γ′ precipitates under superlattice stacking fault formation occurs leading to extreme work hardening rates up to 12 GPa and a total increase in stress of about 200 MPa. Additional investigations on the temperature and strain-rate dependence of the anomalous work hardening behavior reveal the significance of diffusion and segregation processes on the stress-strain curve and the work hardening behavior.

Keywords: superalloy; yielding behavior; work hardening; transmission electron microscopy (TEM); high-temperature deformation

Citation: Bezold, A.; Volz, N.; Xue, F.; Göken, M.; Neumeier, S. Anomalous Work Hardening Behavior of a Single Crystalline Co-Base Superalloy. *Alloys* **2022**, *1*, 243–253. https://doi.org/10.3390/alloys1030015

Academic Editor: Gabriela Vincze

Received: 5 August 2022
Accepted: 20 October 2022
Published: 29 October 2022

1. Introduction

After the discovery of the possibility to strengthen Co-base alloys by coherently embedded γ′ precipitates based on $Co_3(Al,W)$ [1], research groups around the world studied this alloy system regarding the effect of alloying elements, oxidation properties, mechanical properties, and deformation behavior [2–9]. Early investigations by Suzuki et al. revealed that simple ternary and quaternary Co-Al-W(-Ta) alloys exhibit an anomalous increase in the yield strength with increasing temperature [2,3]. Similar to their Ni-base counterparts, this so-called yield strength anomaly (YSA) occurs due to the formation of immobile dislocation configurations through cross-slip processes. While the yield strength of the ternary Co-Al-W drops sharply above the peak temperature as single matrix dislocations are able to bypass the precipitates in combination with a partial dissolution of the γ′ precipitates, the addition of Ta leads to a less pronounced decrease in the yield strength, which is associated with extensive stacking fault (SF) formation inside the γ′ precipitates [3]. In subsequent studies, this effect was confirmed as the transition to extensive stacking fault shearing with increasing temperatures sometimes even led to the maintenance or an increase in the yield strength of some Co-base and CoNi-base superalloys [10–12]. Furthermore, extensive stacking fault formation and frequent interactions between these planar defects also cause high work hardening rates [3,11] and this is also assumed to cause strengthening during creep [13–18]. Since stacking fault shearing is a segregation-assisted process [14,19–26], these strengthening effects, however, are diminished if the temperature becomes too high as their propagation velocity increases and extrinsic stacking faults evolve into microtwins.

In Ni-base superalloys, another interesting yielding behavior was observed and investigated by the group of Mughrabi [27,28]: Distinctive microyielding stages were identified during constant strain-rate tensile tests and correlated to the different stress states inside the superalloy due to the lattice misfit and the arising non-uniform coherency stresses

inside the matrix channels of the alloy CMSX-6. The lattice misfit is defined as the relative difference of the lattice parameter of both the γ and γ' phases:

$$\delta = \frac{a_{\gamma'} - a_{\gamma}}{0.5\left(a_{\gamma'} + a_{\gamma}\right)}, \quad (1)$$

where a_{γ} and $a_{\gamma'}$ are the lattice parameters of the γ and γ' phases, respectively. The negative lattice misfit of CMSX-6 leads to biaxial compressive stresses in the γ matrix channels and triaxial tensile stresses inside the γ' precipitates. After applying an external tensile stress, vertical tensile stresses arise in the horizontal γ channels, while the magnitude of the compressive stresses in the vertical γ channels decreases. As the magnitude of the applied stress increases further, dislocations are able to glide in the horizontal γ channels and form interfacial dislocation networks at the horizontal γ/γ' interfaces leading to the first microyielding stage. Subsequently at higher applied stresses, dislocations shear similarly through the vertical γ channels and form interfacial dislocation networks in the second microyielding stage. The deposited interfacial dislocations can be considered as extra half planes, which are introduced in the γ' precipitates in the horizontal γ channels and in the γ matrix in the vertical γ channels. Due to these extra half-planes, biaxial horizontal tensile stresses and biaxial compressive stresses arise in the horizontal and the vertical γ channels, respectively, which are compensated by inverse stresses in the γ' precipitates. The asymmetric stress state in the γ' precipitates leads to two additional microyielding stages: shearing of the γ/γ' precipitates by dislocation pairs from the horizontal γ/γ' interfaces and at an even higher stress from the vertical γ/γ' interfaces. While these distinctive microyielding stages are clearly observed at 900 °C, they diminish and finally disappear at increasing temperatures due to higher dislocation climb velocities and a faster relaxation of coherency stresses. Similarly, in Co-base superalloys, which have a positive lattice misfit and are deformed under compression, plastic deformation is initiated in the horizontal γ matrix channels [29,30]. However, no distinctive microyielding stages have been reported in this alloy class up to now.

As mentioned above, high work hardening rates were reported in Ta-containing Co-base superalloys, which are associated with extensive stacking fault shearing. A direct correlation between the stress-strain curves associated with this work hardening behavior and the evolution of the underlying defect structure is missing for the otherwise extensively investigated class of Co-Al-W-Ta alloys. The goal of this study is to study the work hardening behavior of a single crystalline Co-Al-W-Ta superalloy via conventional transmission electron microscopy to rationalize the high work-hardening rates in Ta-containing Co-base superalloys. An anomalous work hardening behavior with distinctive microyielding stages is identified and rationalized with the internal stress states and the evolution of the defect structure. Furthermore, the influence of strain-rate and temperature on the occurring deformation mechanisms and the anomalous work hardening behavior is investigated and discussed, which reveals the strengthening and softening effect of stacking fault shearing and microtwinning, respectively.

2. Materials and Methods

The experimental alloy ERBOCo-VF60 (nominal composition: Co-8.9Al-9.0W-2.3Ta (at.%), EDS: Co-8.2Al-9.4W-1.7Ta (at.%)) was produced by a two-step casting process. First, two master alloys were manufactured by MaTeck GmbH (Jülich, Germany) using raw elements of 99.9 wt.% purity. Afterward, both master alloys were mixed in the required ratio, and a single crystal bar with a length of 120 mm and a diameter of 12 mm was cast in a laboratory scale Bridgman unit. More information on the alloy ERBOCo-VF60, henceforth simply referred to as VF60, or the casting process can be found in [31–33].

Since the mechanical properties depend strongly on the crystallographic orientation of the specimens, the single crystalline bar, which was used for the preparation of the compression specimens, was oriented in [001] direction by means of electron backscatter diffraction (EBSD) using a Nordlys detector (Oxford Instruments, Abingdon, United King-

dom) in a Zeiss Crossbeam 1540 EsB (Carl Zeiss, Oberkochen, Germany). After orientation, the deviation from [001] was determined to be 3.1°. For the compression tests, cylindrical specimens with a diameter of 3 mm and a height of 4.5 mm were prepared from the previously oriented segments. Subsequently, the specimens' cylindrical surfaces were ground with SiC abrasive paper with a grit size of at least 1200. For the determination of the yield stress and the analysis of the work hardening behavior, strain-rate-controlled compression tests were carried out using a universal testing machine (Instron 4505 (Instron, Norwood, MA, USA), modified by Hegewald & Peschke (Nossen, Germany)) at various temperatures (850 °C, 950 °C and 1000 °C) and strain-rates (10^{-3} s^{-1}, 10^{-4} s^{-1}, 10^{-5} s^{-1}). From the measured force and displacement data, the engineering stress σ and strain ε are calculated and converted to the true stress $\sigma_t = \sigma(1 + \varepsilon)$ and true strain $\varepsilon_t = \ln(1 + \varepsilon)$. Subsequently, the elastic part of the stress-strain curve is fitted with a linear function and the resulting elastic true strain is subtracted from the true strain to obtain the true plastic strain ε_{pl}. The work hardening rate Θ is determined by $d\sigma_t/d\varepsilon_{pl}$.

The microstructural investigations were conducted using a Philips CM200 (Philips, Eindhoven, The Netherlands) transmission electron microscope (TEM) at a high voltage of 200 kV. The stacking fault nature was determined by the relationship between the fringe contrast in center dark field (CDF) images and the used two-beam conditions. For the TEM analyses, slices with a thickness of approximately 400 µm were first cut from the inner part of the compression specimens. The slices were then carefully ground from both sides with SiC paper (2500 grit size) to a thickness of about 100 µm. They were then further thinned by electropolishing to electron transparency using a Double-Jet *Tenupol-5* (*Struers*) and a solution of 16.7 % nitric acid—83.3% methanol at −25 °C and 40 V.

3. Results

3.1. Mechanical Properties and Deformation Behavior

The stress-strain curves determined at a strain-rate of $1 \cdot 10^{-4}$ s^{-1} and varying temperatures can be seen in Figure 1a. At 850 °C and 950 °C, an increase in the work hardening rate is observed at approximately 1.5 and 2.0% plastic strain, respectively (see also Figure 1c). The peak strength is reached after about 13% and 3% plastic strain in VF60 at 850 °C and 950 °C, respectively, which is followed by softening (negative work hardening rates). At about 13% plastic strain at 950 °C, the alloy suffers failure and the stress quickly drops. Similar to what was reported by Reichstein et al. [27] for the single crystalline Ni-base superalloy CMSX-6, no anomalous work hardening is present at an even higher temperature of 1000 °C. After yielding, there is a rather smooth transition into a continuous softening regime.

Further tests at $1 \cdot 10^{-3}$ s^{-1} and $1 \cdot 10^{-5}$ s^{-1} were carried out at 950 °C. The corresponding stress-strain curves are plotted in Figure 1b. At a strain-rate of $1 \cdot 10^{-3}$ s^{-1}, the material reveals a significantly lower work hardening rate, which starts at a higher plastic strain and extends over a longer strain range, compared to a strain-rate of $1 \cdot 10^{-4}$ s^{-1} as shown in Figure 1d. In contrast, at $1 \cdot 10^{-5}$ s^{-1}, the initial work hardening is much stronger, the maximum strength shifts to a lower plastic strain and the softening afterward is more pronounced than at $1 \cdot 10^{-4}$ $s^{-[1}$ (see Figure 1b).

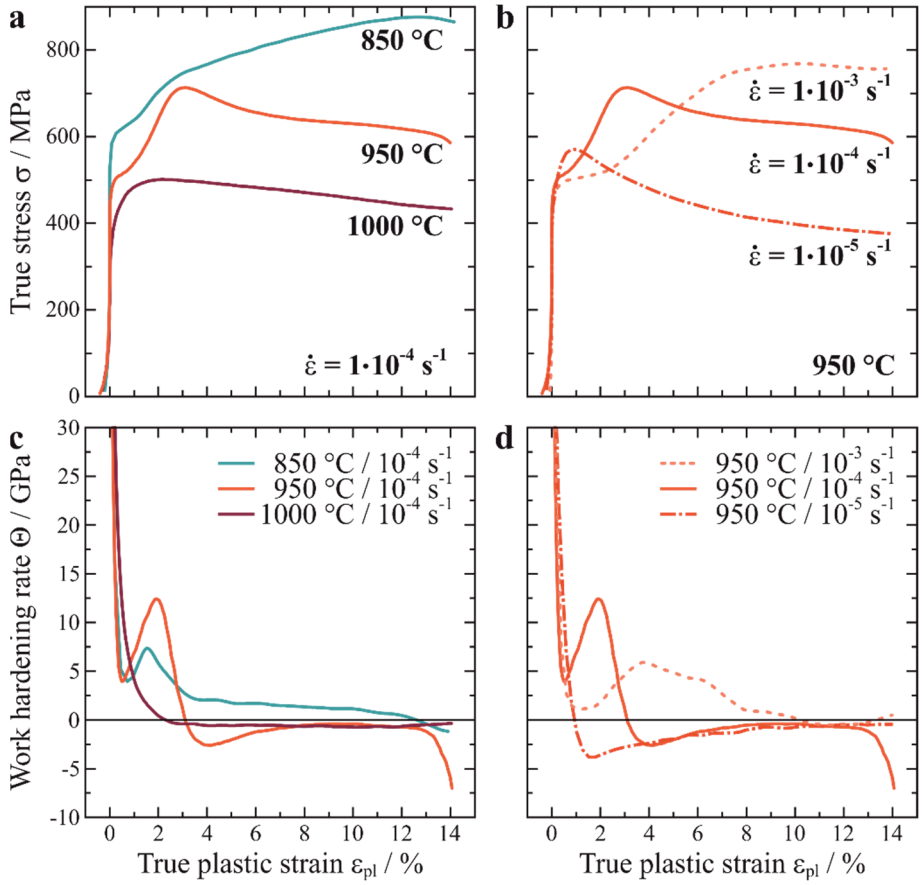

Figure 1. Stress-strain curves of alloy VF60 (**a**) at different temperatures using a strain-rate of $1 \cdot 10^{-4}$ s^{-1}, (**b**) at 950 °C using different strain-rates, and (**c**,**d**) the corresponding work hardening rate curves of (**a**,**b**).

3.2. Microstructure and Deformation Mechanisms

In order to investigate this anomalous work hardening behavior in more detail, TEM investigations were carried out. Compression tests at a strain-rate of $1 \cdot 10^{-4}$ s^{-1} and a temperature of 950 °C were interrupted at characteristic strains, i.e., at the yielding point and the first decrease in work hardening (ε_{pl} ~ 0.2%), at the onset of the strong increase in strength (ε_{pl} ~ 1.1%), and at the maximum stress (ε_{pl} ~ 3.2%), to study the underlying deformation mechanisms.

Figure 2 shows the defect- and microstructure after different levels of strain. The corresponding stress-strain curves of the interrupted specimens are shown in Figure 2a,e,i compared with the uninterrupted curve. At 0.2% plastic strain, the deformation is highly inhomogeneous. While some areas of the specimen are free of defects (Figure 2b), other regions are full of dislocations and stacking faults (Figure 2c). When dislocations cut into the γ' precipitates, the nature of the resulting stacking faults is mostly intrinsic as determined by the fringe contrast criterion in CDF images (Figure 2d). However, in rare cases, superlattice extrinsic stacking faults (SESFs) are also observed but only inside slip bands (Figure 2c). Although the cutting of the precipitates can occasionally be observed, most of the deformation is concentrated in the γ matrix. After further deformation to a plastic strain of about 1.1%, the alloy only slightly hardens. Even after this strain, the deformation is still localized in deformation bands and in the γ matrix phase (Figure 2f–h). However, some dislocation pairs coupled with an anti-phase boundary (APB) are able to shear the γ' precipitates (see white arrows in Figure 2g). APBs created by single superpartial dislocations are also occasionally observed in the γ' precipitates (see white arrows in Figure 2f). In addition, defect configurations could be identified in this condition where

a SISF is coupled with an APB (white dotted arrow in Figure 2g). It was also found that both SISF and SESF are present in the shear bands, while SISFs are still almost exclusively observed outside the bands (Figure 2h). With further deformation up to the maximum stress at about 3.2% plastic strain, the strength increases significantly. The deformation structure reveals that this increase in strength is accompanied by a significant increase in stacking fault density, as can be seen in Figure 2j–l. Furthermore, as additional diffraction reflections appear in TEM diffraction patterns (DPs), it can be assumed that some SESFs have transformed into microtwins. In addition, the microstructural images in Figure 2j–l show that the planar defects interact with each other at different slip planes. Occasionally, APBs generated by single matrix dislocations have also been observed. However, these occur to a much lesser extent compared to SISFs and SESFs and thus their contribution to the overall deformation is negligible. As can be seen in Figure 2l, shear bands with a significantly higher defect density compared to the surrounding areas are still present.

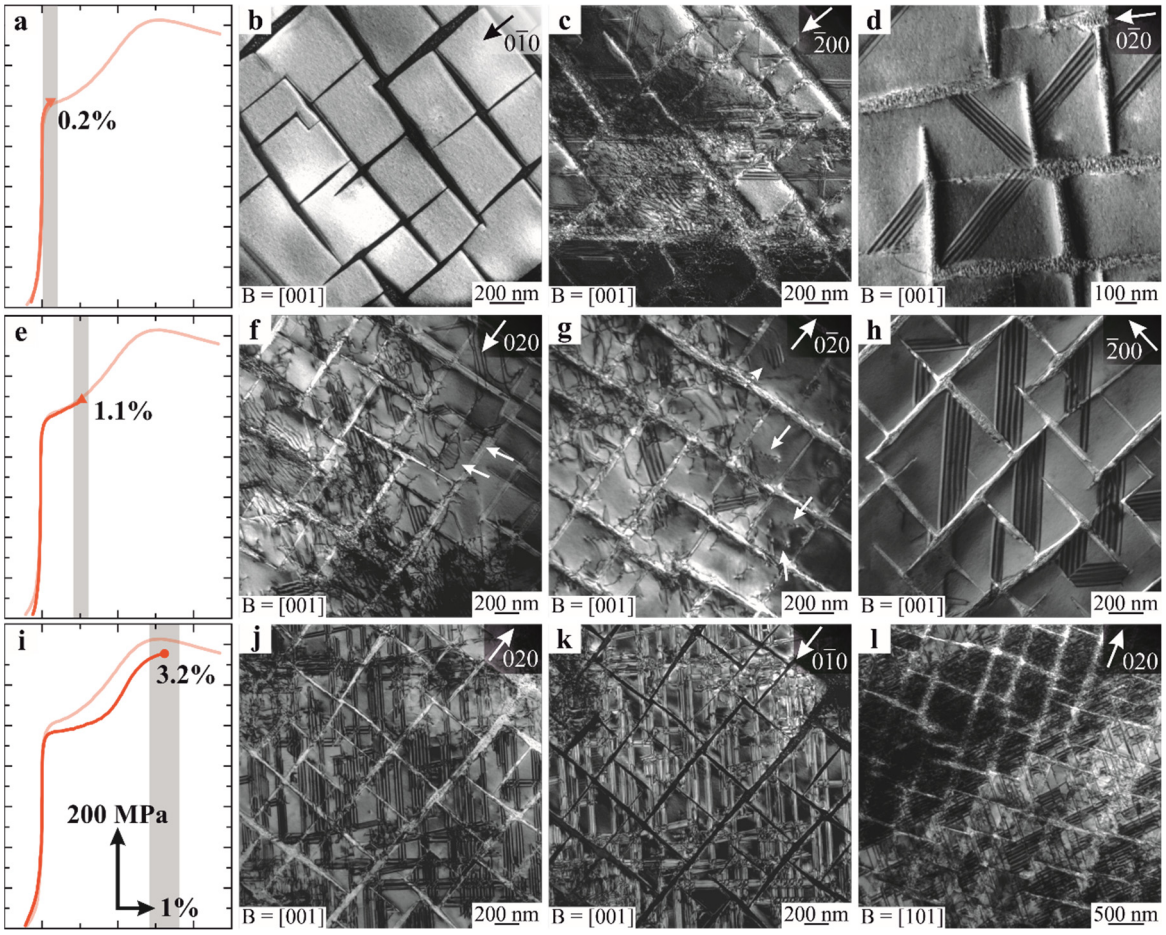

Figure 2. Defect structures in VF60 after compression tests at 950 °C and a strain-rate of $1 \cdot 10^{-4}$ s^{-1} interrupted at (**a**–**d**) 0.2% plastic strain, (**e**–**h**) 1.1% plastic strain and (**i**–**l**) 3.2% plastic strain. The interrupted stress-strain curves are shown in (**a**,**e**,**i**). All TEM micrographs were taken in two-beam conditions close to the [001] zone axis except (l), which was taken close to the [101] zone axis, and with (**f**,**j**,**l**) g = 020 (BF), (**d**,**g**) g = 0–20 (CDF), (**c**,**h**) g = −200 (CDF), and (**b**,**k**) g = 0–10 (CDF).

In order to understand the lower work-hardening rates at a strain-rate of $1 \cdot 10^{-3}$ s^{-1}, an interrupted compression experiment was conducted to a plastic strain of about 3.1 % (Figure 3a). At 3.1% strain, the maximum in the work hardening behavior was found at a strain-rate of $1 \cdot 10^{-4}$ s^{-1}, which does not appear at $1 \cdot 10^{-3}$ s^{-1}. The resulting stacking fault density in the compressed specimen is significantly lower than it is at a strain-rate of $1 \cdot 10^{-4}$ s^{-1} and an identical plastic strain (Figure 3b–d). Because of the reduced density,

the number of interactions between planar faults on different glide planes also decreases substantially. These stacking faults are identified to be SISFs as well as SESFs by comparing the fringe contrast in BF/CDF image pairs (Figure 3b,c). No additional spots in the DP were observed in the [101] viewing direction indicating the absence of microtwinning. Instead, more APB-coupled dislocation pairs and single APBs generated by matrix dislocations (white dotted and continuous arrows in Figure 3b) can be observed. Finally, pronounced dislocation activity in the γ channels is locally observed as shown in Figure 3d.

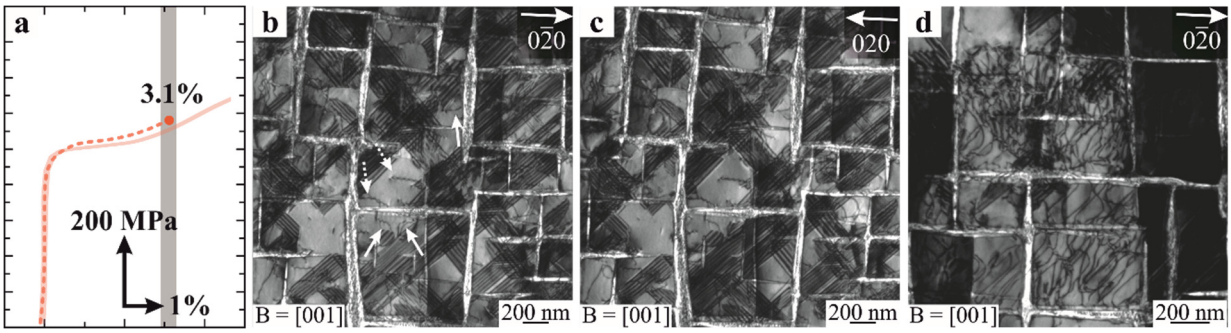

Figure 3. Defect structures in VF60 after a compression test at 950 °C and a strain-rate of $1 \cdot 10^{-3}$ s^{-1} interrupted at a plastic strain of 3.1%. The interrupted stress-strain curve is shown in (**a**). All TEM micrographs were taken in two-beam conditions close to the [001] zone axis and with (**b**,**d**) g = 0–20 (BF) and (**c**) g = 020 (CDF).

In order to investigate why no anomalous work hardening behavior occurs at lower strain-rates and/or higher temperatures, an additional sample was interrupted at about 1.3% plastic strain at 1000 °C and a strain-rate of $1 \cdot 10^{-4}$ s^{-1} (Figure 4a), which corresponds to the peak stress at this temperature and strain-rate. Superlattice stacking fault (SSF) shearing-induced plasticity is the dominant shearing mechanism for VF60 at 1000 °C as shown in Figure 4b,c. These SSFs are of approximately equally intrinsic or extrinsic character as shown in the CDF image in Figure 4b. The variability in the thickness of the edge-on SSFs (Figure 4c) as well as the additional diffraction spot in the corresponding DP indicate the existence of microtwins. Although deformation is spread more homogeneously across the microstructure, shearing events are locally predominantly active on only one {111} glide plane. While shearing by APB-coupled dislocation pairs is nearly absent, single perfect matrix dislocations are able to shear into the γ' precipitates as marked by the white arrows in Figure 4d. The resulting APBs are curved indicating migration from {111} to {001} planes.

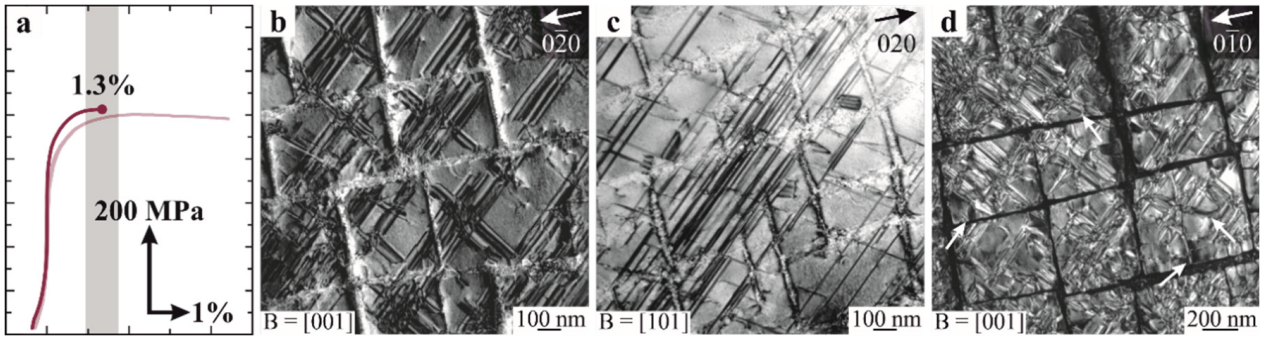

Figure 4. Defect structures in VF60 after compression tests at 1000 °C and a strain-rate of $1 \cdot 10^{-4}$ s^{-1} interrupted at a plastic strain of 1.3%. The interrupted stress-strain curve are shown in (**a**). All TEM micrographs were taken in two-beam conditions close to the (**b**,**d**) [001] or (**c**) [101] zone axis and with (**b**) g = 0–20 (CDF), (**c**) g = 020 (BF) and (**d**) g = 0–10 (CDF).

4. Discussion

The correlation of the defect structures in VF60 after the interrupted compression experiments with the anomalous work-hardening behavior at 950 °C and a strain-rate of 10^{-4} s^{-1} revealed that the strong increase in the work-hardening rate is directly associated with an increasing stacking fault density and numerous interactions between these planar faults.

In the literature, an anomalous work hardening behavior has also been observed in Ni-base superalloys at 900 °C as mentioned in the introduction. Reichstein et al. [27] found such a behavior in tensile tests on the alloy CMSX-6 and related it to the asymmetric stress state in the γ matrix and the γ' precipitates. While a similar behavior is also found in VF60, only one distinct stage arose in the range of 1–2% plastic strain (see Figure 1) compared to the four distinct stages observed in CMSX-6 [27]. Nevertheless, it can still be assumed that the deformation mechanisms and the movement of dislocations are crucial for the anomalous work hardening behavior here as well. Based on the work of Reichstein et al. [27] and the CTEM investigations, the reasons for this anomalous work hardening behavior are rationalized in the following.

The investigation of the underlying defect structures shown in Figure 2 revealed that deformation essentially takes place in the horizontal γ matrix channels after a plastic deformation of approximately 0.2% (Figure 5a). This is in accordance with theoretical predictions: Due to the positive lattice misfit of VF60 [29], biaxial tensile stresses and triaxial compressive stresses arise inside the γ channels and the γ' precipitate, respectively. As the external compressive load is applied, the superposition of the coherency and the applied stress leads to higher effective compressive stresses inside the horizontal than in the vertical γ channels as indicated by the red arrows in Figure 5b. This facilitates dislocation movement in the horizontal γ channels and the deposition of dislocations at the horizontal γ/γ' interfaces. Similar observations were also made in a similar alloy during the early stages of compressive creep deformation at 950 °C and an applied load of 150 MPa [29,30]. Occasionally, the formation of a small number of SISFs created by partial dislocations shearing through the γ' phase (less than one stacking fault per γ' precipitate) was also observed.

At this deformation stage, the work hardening rate is comparatively low and the increase in strength is due to the increase in dislocation density in the matrix. As strain increases, other deformation mechanisms occur (Figure 5c,d): shearing by APB-coupled pairs of $a/2 < 110 >$ type superpartial dislocations, by single superpartial dislocations, and under stacking faults, which are connected to APBs. However, the contribution of the latter two mechanisms is estimated to be negligible, as both extend over only very short distances into the precipitates and are only observed occasionally. Most of the superpartial dislocation pairs have not yet formed sessile Kear-Wilsdorf locks and can freely move through the microstructure. This could explain why the strain hardening rate after 1.1% strain is still comparatively moderate. Even though the dislocation density is slightly increased in the vertical and horizontal γ channels, deformation generally takes place in a highly heterogeneous manner on deformation bands even in this condition. After the stress plateau region, deformation proceeds mainly by extensive SSF-based shearing up to the peak stress state. The increase in dislocation density in the γ matrix leads to an impediment in the movement of matrix dislocations. Presumably, the segregation of alloying elements to the dislocations located at the γ/γ' interface facilitates cutting into the γ' phase, resulting in a significant increase in stacking fault density [11,25,26]. The interaction of stacking faults with each other can then lead to a significant increase in strength [11,15–18]. However, single microtwins have also been observed. The formation of these microtwins together with the increasing degradation of the microstructure then probably leads to the subsequent decrease in strength. Thus, the change in deformation mechanisms appears to be responsible for the anomalous work hardening behavior of VF60.

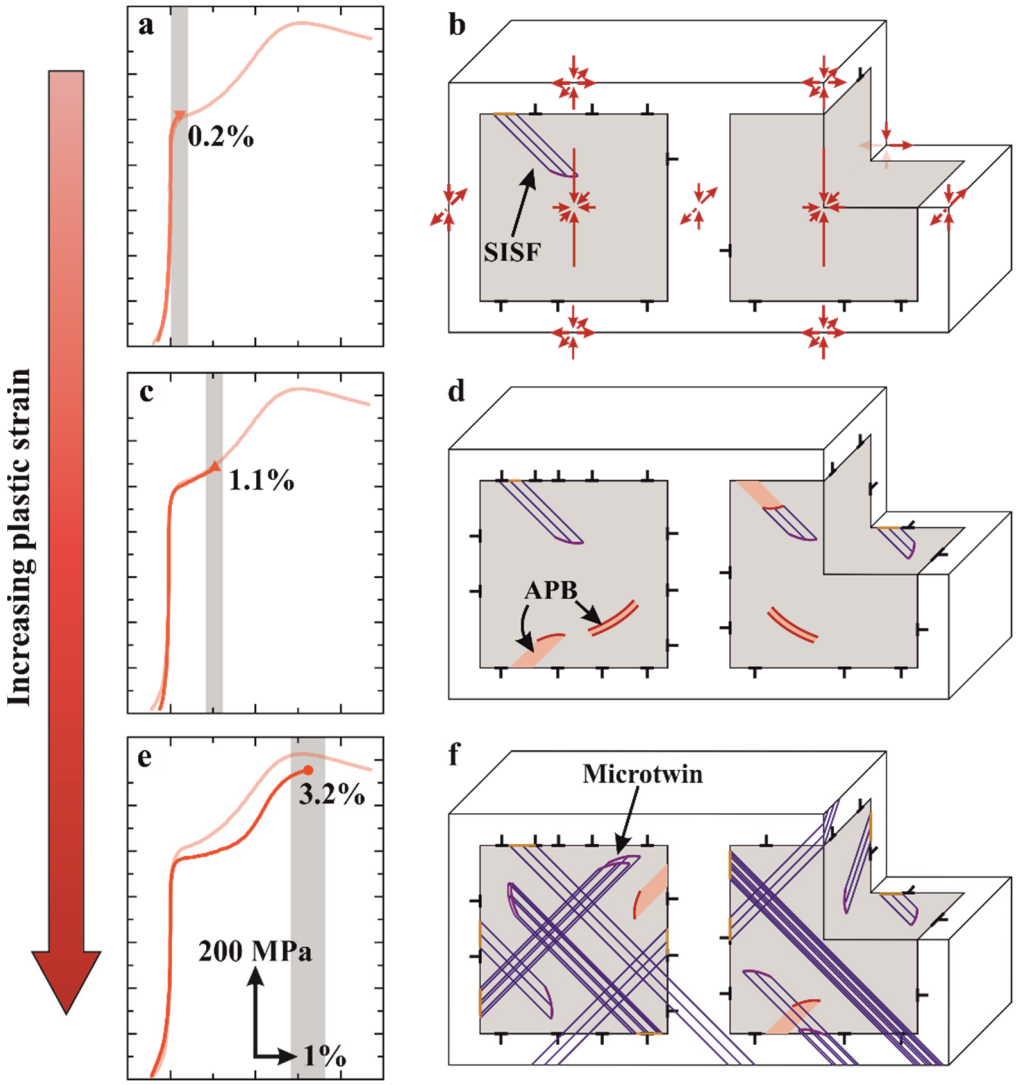

Figure 5. Schematic drawings of the evolution of the defect structure in VF60 at 950 °C; (**b**) Initially deformation starts in the horizontal γ channels; although, SISFs are occasionally observed in the γ′ precipitates. The superposition of the misfit stresses with the external stress is indicated; (**d**) With increasing plastic strain, deformation is still mainly confined to the γ channels. However, multiple shearing mechanisms are also active: shearing by APB-coupled dislocation pairs, by single super-partial dislocations, and by stacking faults connected to APBs. (**f**) After the γ matrix channels are filled, massive SSF-based shearing occurs, which also leads to the formation of microtwins and is the reason for the high work hardening. In (**a**,**c**,**e**), the stress-strain curves up to the discussed strain level are shown.

It has already been explained above that a similar behavior could also be observed in Ni-base superalloys [27]. There, it could be shown that this effect disappears with increasing temperature due to higher climb velocities and a quicker relaxation of the coherency stresses and thus the asymmetric stress state [27]. Even though the mechanism for the anomalous strain hardening behavior of VF60 is different, the temperature effect was also investigated in this work.

As shown previously, the significance of stacking fault shearing varies strongly with temperature [11]. At a lower temperature of 850 °C, diffusion processes are slower and segregation-assisted stacking fault shearing is most likely not as dominant and their interactions not as frequent as at higher temperatures. Thus, the intermediate work hardening rate is lower than at 950 °C, as shown in Figure 1c. On the other hand, the lower diffusion

rate decreases the propensity to microstructural degradation processes and microtwinning, which leads to a larger work hardening regime up to a plastic strain of 13%. Conversely, at a temperature of 1000 °C, diffusion and segregation to defects can proceed even faster than at 950 °C, which shifts the peak stress to lower plastic strain values and thus shorter test times.

A similar impact of diffusion-assisted shearing of the γ' phase by partial dislocations on the creep behavior of a similar Co-Al-W-Ta alloy was recently found by Volz et al. [25]. There, the intermediate softening due to the cutting of γ' was also shifted to shorter test times at higher temperatures, since the faster segregation of Ta and W to dislocations and stacking faults facilitated the shearing processes. The absence of the anomalous work hardening behavior at 1000 °C here can then probably be explained by a combination of two effects: First, it can be assumed that thermally activated matrix deformation processes, i.e., dislocation climb and cross-slip, are also accelerated in VF60, as has also been observed in CMSX-6, at higher temperatures [27]. This leads to a reduction in the hardening contribution by stacking fault interactions, as fewer dislocations are required to cut into the precipitation phase to realize the experimentally set strain-rate. Second, the faster diffusion facilitates the segregation of alloying elements to interfacial dislocations after even shorter times, which probably smears out the effect of a strength increase with the initial range of the stress-strain curve. Furthermore, the comparatively faster segregation at intersections of stacking faults further weakens their hardening contribution and a higher diffusion rate leads to an easier dislocation motion in γ'. Both of these factors contribute to the shift in the anomalous strength increase to lower strains or its non-appearance. This assumption that a time-dependent effect based on the diffusion of alloying elements plays a decisive role is further validated by the investigations of varying strain-rates on the anomalous work hardening behavior. At higher strain-rates, less time is available for the diffusion and segregation of alloying elements, and thus higher plastic strain values are required to reach similar stacking fault densities. Accordingly, the work hardening rates are decreased but extend over a larger plastic strain regime. Conversely, this means that at lower strain-rates, an increased density of stacking faults and thus the maximum strength already occur at very low strains, because there has been enough time for diffusion and segregation. However, microtwinning and microstructural degradation processes then also start at lower strains, such that the stress drops continuously after reaching the maximum. These investigations undoubtedly reveal the strengthening and softening effects of stacking fault shear and microtwinning, respectively. As shown by Smith et al. [20,34], microtwinning can be inhibited by local phase transformations along the stacking faults. Thus, the strengthening effect provided by stacking fault shearing might be used in future alloys, which simultaneously inhibit microtwinning, and, thus, exhibit superior mechanical properties at high temperatures.

5. Conclusions

In this work, the anomalous work hardening behavior of the Co-base superalloy alloy VF60 (Co-8.9Al-9.0W-2.3Ta) was investigated by compression testing at different temperatures and strain-rates. The following conclusions can be drawn:

- The anomalous work hardening behavior at 950 °C and a strain-rate of 10^{-4} s^{-1} with a strength increase of approximately 200 MPa within only 3% plastic deformation are due to a change in deformation mechanism from dislocation motion in the γ matrix to extensive stacking fault formation in the γ' precipitates, which then interact with each other and thus increase the strength.
- Since shearing of dislocations into the γ' precipitates is facilitated by segregation, diffusion plays an important role. The significant increase in the work hardening rate and the corresponding maximum stress is reached at lower plastic strains at both higher temperatures and lower strain-rates, since segregation can occur more quickly in each case.

- At lower temperatures (850 °C) or higher temperatures (1000 °C) no (distinct) intermediate increase in the work hardening behavior occurs. While diffusion is either too slow so that the segregation of alloying elements may be less pronounced or take too much time at lower temperatures, the situation is reversed at too high temperatures as segregation occurs too quickly, weakening the hardening contribution of stacking faults, increasing the dislocation velocity, and facilitating microtwinning and microstructural degradation processes.

Author Contributions: Conceptualization, A.B., N.V., and S.N.; Formal analysis, A.B. and N.V.; Funding acquisition, M.G. and S.N.; Investigation, A.B. and N.V.; Methodology, A.B.; Project administration, S.N.; Supervision, M.G. and S.N.; Visualization, A.B.; Writing—original draft, A.B., N.V., and S.N.; Writing—review and editing, N.V., F.X., M.G., and S.N. All authors have read and agreed to the published version of the manuscript.

Funding: This research was funded by the Deutsche Forschungsgemeinschaft (DFG) through projects B3 and Z01 of the collaborative research center SFB/TR 103 on single crystal superalloys.

Institutional Review Board Statement: Not applicable.

Informed Consent Statement: Not applicable.

Data Availability Statement: The research data are available from the corresponding author on request.

Acknowledgments: The authors acknowledge funding by the Deutsche Forschungsgemeinschaft (DFG) through projects B3 and Z01 of the collaborative research center SFB/TR 103 on single crystal superalloys.

Conflicts of Interest: The authors declare no conflict of interest.

References

1. Sato, J.; Omori, T.; Oikawa, K.; Ohnuma, I.; Kainuma, R.; Ishida, K. Cobalt-Base High-Temperature Alloys. *Science* **2006**, *312*, 90–91. [CrossRef] [PubMed]
2. Suzuki, A.; DeNolf, G.C.; Pollock, T.M. Flow stress anomalies in γ/γ' two-phase Co–Al–W-base alloys. *Scr. Mater.* **2007**, *56*, 385–388. [CrossRef]
3. Suzuki, A.; Pollock, T.M. High-temperature strength and deformation of γ/γ' two-phase Co–Al–W-base alloys. *Acta Mater.* **2008**, *56*, 1288–1297. [CrossRef]
4. Bauer, A.; Neumeier, S.; Pyczak, F.; Göken, M. Microstructure and creep strength of different γ/γ'-strengthened Co-base superalloy variants. *Scr. Mater.* **2010**, *63*, 1197–1200. [CrossRef]
5. Klein, L.; Shen, Y.; Killian, M.S.; Virtanen, S. Effect of B and Cr on the high temperature oxidation behaviour of novel γ/γ'-strengthened Co-base superalloys. *Corros. Sci.* **2011**, *53*, 2713–2720. [CrossRef]
6. Xue, F.; Wang, M.; Feng, Q. Alloying Effects on Heat-Treated Microstructure in Co-Al-W-Base Superalloys at 1300 °C and 900 °C. In *Superalloys 2012*; TMS: Warrendale, PA, USA, 2012; pp. 813–821, ISBN 978-1-118-51643-0.
7. Titus, M.S.; Suzuki, A.; Pollock, T.M. Creep and directional coarsening in single crystals of new γ–γ' cobalt-base alloys. *Scr. Mater.* **2012**, *66*, 574–577. [CrossRef]
8. Meher, S.; Yan, H.-Y.; Nag, S.; Dye, D.; Banerjee, R. Solute partitioning and site preference in γ/γ' cobalt-base alloys. *Scr. Mater.* **2012**, *67*, 850–853. [CrossRef]
9. Klein, L.; Killian, M.S.; Virtanen, S. The effect of nickel and silicon addition on some oxidation properties of novel Co-based high temperature alloys. *Corros. Sci.* **2013**, *69*, 43–49. [CrossRef]
10. Bezold, A.; Volz, N.; Lenz, M.; Zenk, C.H.; Spiecker, E.; Mills, M.; Göken, M.; Neumeier, S. Yielding behavior of a single-crystalline γ'-strengthened Co-Ti-Cr superalloy. *Scr. Mater.* **2021**, *200*, 113928. [CrossRef]
11. Bezold, A.; Volz, N.; Lenz, M.; Karpstein, N.; Zenk, C.H.; Spiecker, E.; Göken, M.; Neumeier, S. Quantification of the temperature-dependent evolution of defect structures in a CoNi-base superalloy. *Acta Mater.* **2022**, *227*, 117702. [CrossRef]
12. Cao, B.X.; Xu, W.-W.; Yu, C.Y.; Wu, S.W.; Kong, H.J.; Ding, Z.Y.; Zhang, T.L.; Luan, J.H.; Xiao, B.; Jiao, Z.B.; et al. L12-strengthened multicomponent Co-Al-Nb-based alloys with high strength and matrix-confined stacking-fault-mediated plasticity. *Acta Mater.* **2022**, *229*, 117763. [CrossRef]
13. Xue, F.; Zhou, H.J.; Shi, Q.Y.; Chen, X.H.; Chang, H.; Wang, M.L.; Feng, Q. Creep behavior in a γ' strengthened Co–Al–W–Ta–Ti single-crystal alloy at 1000 °C. *Scr. Mater.* **2015**, *97*, 37–40. [CrossRef]
14. Titus, M.S.; Mottura, A.; Babu Viswanathan, G.; Suzuki, A.; Mills, M.J.; Pollock, T.M. High resolution energy dispersive spectroscopy mapping of planar defects in L12-containing Co-base superalloys. *Acta Mater.* **2015**, *89*, 423–437. [CrossRef]
15. Zhou, H.J.; Chang, H.; Feng, Q. Transient minimum creep of a γ' strengthened Co-base single-crystal superalloy at 900 °C. *Scr. Mater.* **2017**, *135*, 84–87. [CrossRef]

16. Lu, S.; Antonov, S.; Li, L.; Feng, Q. Two Steady-State Creep Stages in Co-Al-W-Base Single-Crystal Superalloys at 1273 K/137 MPa. *Metall. Mater. Trans. A* **2018**, *49*, 4079–4089. [CrossRef]
17. Lu, S.; Antonov, S.; Li, L.; Liu, C.; Zhang, X.; Zheng, Y.; Fraser, H.L.; Feng, Q. Atomic structure and elemental segregation behavior of creep defects in a Co-Al-W-based single crystal superalloys under high temperature and low stress. *Acta Mater.* **2020**, *190*, 16–28. [CrossRef]
18. Zhou, H.; Li, L.; Antonov, S.; Feng, Q. Sub/micro-structural evolution of a Co–Al–W–Ta–Ti single crystal superalloy during creep at 900 °C and 420 MPa. *Mater. Sci. Eng. A* **2020**, *772*, 138791. [CrossRef]
19. Viswanathan, G.B.; Shi, R.; Genc, A.; Vorontsov, V.A.; Kovarik, L.; Rae, C.M.F.; Mills, M.J. Segregation at stacking faults within the γ' phase of two Ni-base superalloys following intermediate temperature creep. *Scr. Mater.* **2015**, *94*, 5–8. [CrossRef]
20. Smith, T.M.; Esser, B.D.; Antolin, N.; Viswanathan, G.B.; Hanlon, T.; Wessman, A.; Mourer, D.; Windl, W.; McComb, D.W.; Mills, M.J. Segregation and η phase formation along stacking faults during creep at intermediate temperatures in a Ni-based superalloy. *Acta Mater.* **2015**, *100*, 19–31. [CrossRef]
21. Eggeler, Y.M.; Müller, J.; Titus, M.S.; Suzuki, A.; Pollock, T.M.; Spiecker, E. Planar defect formation in the γ' phase during high temperature creep in single crystal CoNi-base superalloys. *Acta Mater.* **2016**, *113*, 335–349. [CrossRef]
22. Barba, D.; Pedrazzini, S.; Vilalta-Clemente, A.; Wilkinson, A.J.; Moody, M.P.; Bagot, P.A.J.; Jérusalem, A.; Reed, R.C. On the composition of microtwins in a single crystal nickel-based superalloy. *Scr. Mater.* **2017**, *127*, 37–40. [CrossRef]
23. Makineni, S.K.; Kumar, A.; Lenz, M.; Kontis, P.; Meiners, T.; Zenk, C.; Zaefferer, S.; Eggeler, G.; Neumeier, S.; Spiecker, E.; et al. On the diffusive phase transformation mechanism assisted by extended dislocations during creep of a single crystal CoNi-based superalloy. *Acta Mater.* **2018**, *155*, 362–371. [CrossRef]
24. He, J.; Zenk, C.H.; Zhou, X.; Neumeier, S.; Raabe, D.; Gault, B.; Makineni, S.K. On the atomic solute diffusional mechanisms during compressive creep deformation of a Co-Al-W-Ta single crystal superalloy. *Acta Mater.* **2020**, *184*, 86–99. [CrossRef]
25. Volz, N.; Xue, F.; Zenk, C.H.; Bezold, A.; Gabel, S.; Subramanyam, A.P.A.; Drautz, R.; Hammerschmidt, T.; Makineni, S.K.; Gault, B.; et al. Understanding creep of a single-crystalline Co-Al-W-Ta superalloy by studying the deformation mechanism, segregation tendency and stacking fault energy. *Acta Mater.* **2021**, *214*, 117019. [CrossRef]
26. Barba, D.; Alabort, E.; Pedrazzini, S.; Collins, D.M.; Wilkinson, A.J.; Bagot, P.A.J.; Moody, M.P.; Atkinson, C.; Jérusalem, A.; Reed, R.C. On the microtwinning mechanism in a single crystal superalloy. *Acta Mater.* **2017**, *135*, 314–329. [CrossRef]
27. Reichstein, S.; Kraft, S.; Mughrabi, H. Sequence of distinct microyielding stages of the monocrystalline nickel-base superalloy CMSX-6 at high temperatures. *Int. J. Mater. Res.* **2009**, *100*, 494–499. [CrossRef]
28. Mughrabi, H. Microstructural aspects of high temperature deformation of monocrystalline nickel base superalloys: Some open problems. *Mater. Sci. Technol.* **2009**, *25*, 191–204. [CrossRef]
29. Xue, F.; Zenk, C.H.; Freund, L.P.; Hoelzel, M.; Neumeier, S.; Göken, M. Double minimum creep in the rafting regime of a single-crystal Co-base superalloy. *Scr. Mater.* **2018**, *142*, 129–132. [CrossRef]
30. Xue, F.; Zenk, C.H.; Freund, L.P.; Neumeier, S.; Göken, M. Understanding raft formation and precipitate shearing during double minimum creep in a γ'-strengthened single crystalline Co-base superalloy. *Philos. Mag.* **2021**, *101*, 326–353. [CrossRef]
31. Bezold, A.; Volz, N.; Xue, F.; Zenk, C.H.; Neumeier, S.; Göken, M. On the Precipitation-Strengthening Contribution of the Ta-Containing Co_3(Al,W)-Phase to the Creep Properties of γ/γ' Cobalt-Base Superalloys. *Metall. Mater. Trans. A* **2020**, *51*, 1567–1574. [CrossRef]
32. Volz, N.; Xue, F.; Bezold, A.; Zenk, C.H.; Fries, S.G.; Schreuer, J.; Neumeier, S.; Göken, M. Design of a Co–Al–W–Ta Alloy Series with Varying γ' Volume Fraction and Their Thermophysical Properties. *Metall. Mater. Trans. A* **2021**, *52*, 3931–3944. [CrossRef]
33. Heckl, A.; Rettig, R.; Singer, R.F. Solidification Characteristics and Segregation Behavior of Nickel-Base Superalloys in Dependence on Different Rhenium and Ruthenium Contents. *Metall. Mater. Trans. A* **2010**, *41*, 202. [CrossRef]
34. Smith, T.M.; Esser, B.D.; Antolin, N.; Carlsson, A.; Williams, R.E.A.; Wessman, A.; Hanlon, T.; Fraser, H.L.; Windl, W.; McComb, D.W.; et al. Phase transformation strengthening of high-temperature superalloys. *Nat. Commun.* **2016**, *7*, 13434. [CrossRef] [PubMed]